

PACS numbers: 52.57. – z; 52.38.Ph; 42.55.Ks
DOI: 10.1070/QE2007v037n04ABEH013219

Numerical simulation of three-dimensional X-ray and laser field inhomogeneities in experiments with spherical box converters on the Iskra-5 facility

S.V. Bondarenko, G.V. Dolgoleva, E.A. Novikova

Abstract. **The results of spectral calculations of the dynamics of laser radiation absorption and X-ray generation in a spherical box converter are presented for experiments on inertial fusion performed in the 1990s on the Iskra-5 facility. Numerical simulations were carried out taking into account the actual configuration of 12 laser beams and six apertures for introducing laser radiation. Calculations were performed in the sector approximation in which the inner surface of the box is divided into a certain number of regions or sectors. The movement of matter and radiation transport in each sector were calculated by using the one-dimensional spectral non-equilibrium dynamics program. Spectral calculations showed a strong inhomogeneity of irradiation of a capsule in the *M*-band region (2.7 – 2.9 keV). It is shown that the spectrum-averaged root-mean-square inhomogeneity of the X-ray energy flux on the capsule (during the time of its compression) is about 2.5 % for laser beams of the same energy and is about 3 % if the characteristic energy misbalance between the beams is taken into account.**

Keywords: *interaction of laser radiation with matter, laser fusion.*

1. Introduction

During the 1990s, a series of laser fusion experiments were performed on the Iskra-5 facility at the Russian Federal Nuclear Center 'All-Russian Scientific Research Institute of Experimental Physics' in Sarov [1 – 2]. In these experiments, capsules containing a thermonuclear fuel (a gaseous mixture of deuterium and tritium) were irradiated by quasi-equilibrium X-rays generated in a box converter following the absorption of high-power laser radiation introduced in it. Under the action of radiation with the effective temperature $T_X \approx 200$ eV, part of the material of the capsule shell is vaporised and forms a pressure pulse which compresses the thermonuclear fuel. Such an action of radiation is referred to as indirect irradiation of the target. Targets with spherical and cylindrical symmetry of the box were used in the experiments. In this study, we shall confine our analysis to the spherical geometry of the box.

S.V. Bondarenko, G.V. Dolgoleva, E.A. Novikova Russian Federal Nuclear Center 'All-Russian Scientific Research Institute of Experimental Physics', prosp. Mira 37, 607190 Sarov, Nizhegorodskaya region, Russia; e-mail: dolg@vniief.ru

Received 25 April 2006; revision received 10 October 2006
Kvantovaya Elektronika **37** (4) 372 – 378 (2007)
Translated by Ram Wadhwa

The most important problem is to achieve a high uniformity of the capsule surface irradiation required for the uniform compression of a thermonuclear fuel. The uniformity of the X-ray field on the capsule is determined by the parameters of the X-ray source at the box converter walls. The inhomogeneity of radiation of the box walls is caused by the box design (for example, its geometry), but is determined mainly by the inhomogeneity of the laser radiation absorption distribution (i.e. by the position of primary laser spots and secondary redistribution of laser radiation multiply reflected inside the box).

In a number of papers (see, for example, [3 – 5]), the X-ray generation dynamics in vacuum cavities was calculated on the basis of self-similar solutions obtained in [6]. In this approach, the cavity surface is divided into elements, and the visibility factors of all the remaining surface elements are calculated for each of them. The X-ray luminosity of various elements is determined by solving a nonlinear system of algebraic equations. The results of three-dimensional calculations of X-ray generation in a spherical box converter with four apertures (arranged in the tetrahedral symmetry) on the OMEGA facility are presented in [7]. The X-ray luminosity of various elements of the inner surface of the box was obtained by solving the single-group diffusion equation taking into account heating due to the absorption of incident laser radiation, intrinsic radiation energy losses, and the X-rays from the remaining sectors of the inner surface of the box. We developed an approach based on a series of sector calculations using the spectral nonequilibrium dynamics (SND) program [8]. This technique makes it possible to perform one-dimensional calculations of the two-temperature gas dynamics and radiation transport (in the multigroup diffusion approximation). Each of the sector calculations was performed independently, and the boundary conditions for X-ray and laser radiation were used for establishing a connection between the results of calculations.

In the SND program, the following system of partial differential equations is used: the equation of motion

$$\frac{\mathrm{d}u}{\mathrm{d}t} = -r^{\vartheta}\frac{\partial(P_\mathrm{e}+P_\mathrm{i}+P_\mathrm{rad}+\varepsilon)}{\partial m} + r^{\vartheta}\frac{\partial}{\partial m}\left[\rho\beta\frac{\partial(r^{\vartheta}u)}{\partial m}\right] - \frac{3}{2}\vartheta r^{\vartheta-1}\frac{\partial\beta}{\partial m}u \qquad (1)$$

taking viscosity into account, the continuity equation

$$\frac{\mathrm{d}}{\mathrm{d}t}\left(\frac{1}{\rho}\right) = \frac{\partial}{\partial m}(r^{\vartheta}u), \qquad (2)$$

the equation

$$\frac{\mathrm{d}r}{\mathrm{d}t} = u \tag{3}$$

for recalculating the Euler coordinate, the equation

$$\frac{\mathrm{d}E_\mathrm{e}}{\mathrm{d}t} = -P_\mathrm{e}\frac{\partial}{\partial m}\left(r^\vartheta u\right) + \frac{c}{\rho}\int_0^\infty \left(\chi_\omega^\mathrm{abs}U_\omega - \chi_\omega^\mathrm{rad}U_{\omega\,\mathrm{eq}}\right)\mathrm{d}\omega$$

$$+ \frac{1}{l_0\rho}\int_0^\infty J_\omega \mathrm{d}\omega + C_\mathrm{rel}(T_\mathrm{i} - T_\mathrm{e}) - \frac{\partial W_\mathrm{e}}{\partial m} + Q^{(T)} \tag{4}$$

describing the change in the electron component energy, the radiation transport equation

$$\frac{1}{c}\frac{\partial U_\omega}{\partial t} - \frac{1}{r^{(\vartheta)}}\frac{\partial}{\partial r}\left(r^\vartheta S_\omega\right) + \frac{P_\mathrm{rad}}{c}\frac{\partial}{\partial r}\left(r^\vartheta u\right)$$

$$= \frac{\omega}{l_0}\frac{\partial}{\partial\omega}J_\omega - \chi_\omega^\mathrm{abs}U_\omega + \chi_\omega^\mathrm{rad}U_{\omega\,\mathrm{eq}}, \tag{5}$$

in which

$$J_\omega = b(\omega, T_\mathrm{e})\frac{\partial}{\partial\omega}\left(\frac{U_\omega}{\omega^3}\right) + a(\omega, T_\mathrm{e})\frac{U_\omega}{\omega^3}, \tag{6}$$

and

$$S_\omega = -\frac{1}{\chi_\omega}\frac{\partial}{\partial r}\left(\frac{1}{3}U_\omega\right), \tag{7}$$

the ionisation kinetics equation

$$\frac{1}{\rho}\frac{\mathrm{d}}{\mathrm{d}t}\left(\rho P_n^{(i)}\right) = R_n^{(i)}G_n^{(i)}N_\mathrm{e} - I_n^{(i)}P_n^{(i)}N_\mathrm{e}$$

$$+\sum_{m>n}\left[A_{nm}^{(i)}P_m^{(i)}G_n^{(i)} + N_\mathrm{e}\left(C_{mn}^{D(i)}P_m^{(i)}G_n^{(i)} - C_{nm}^{U(i)}P_n^{(i)}G_m^{(i)}\right)\right]$$

$$-\sum_{m<n}\left[A_{nm}^{(i)}P_n^{(i)}G_m^{(i)} + N_\mathrm{e}\left(C_{nm}^{D(i)}P_n^{(i)}G_m^{(i)} - C_{mn}^{U(i)}P_m^{(i)}G_n^{(i)}\right)\right] \tag{8}$$

in the mean-ion approximation, and the equations of state

$$E_\mathrm{e} = E_\mathrm{e}\left(\rho, T_\mathrm{e}, P_n^{(i)}\right), \quad E_\mathrm{i} = E_\mathrm{i}\left(\rho, T_\mathrm{i}, P_n^{(i)}\right),$$

$$P_\mathrm{e} = P_\mathrm{e}\left(\rho, T_\mathrm{e}, P_n^{(i)}\right), \quad P_\mathrm{i} = P_\mathrm{i}\left(\rho, T_\mathrm{i}, P_n^{(i)}\right) \tag{9}$$

supplementing the system. The following notation has been used in the above equations: t is the time; ϑ is the symmetry index ($\vartheta = 2$, 1 and 0 correspond to spherical, cylindrical and plane symmetry, respectively); u is the gasdynamic velocity of matter; r is the Euler radius of a point; ρ is the density of the substance; $m = \int_0^r r^\vartheta \rho \mathrm{d}r$ is its mass; E_e, E_i, T_e, T_i, P_e, and P_i are the internal specific energy, temperature and pressure of electrons and ions, respectively; β is the physical viscosity; ε is the mathematical viscosity; C_rel is the coefficient of relaxation between electrons and ions; $Q^{(T)}$ is the energy absorbed due to the braking mechanism; W_e is the thermal conductivity flux; c is the speed of light; ω is the frequency; U_ω is the spectral density of radiation; $U_{\omega eq}$ is the spectral density of equilibrium radiation; χ_ω^abs and χ_ω^rad are the spectral coefficients of absorption and radiation, respectively; l_0 is a constant; $a(\omega, T_\mathrm{e})$ and $b(\omega, T_\mathrm{e})$ are the coefficients of photon transition from one energy group to another; $P_n^{(i)}$ is the population density of the nth ($n = 1 - N_\mathrm{max}$) level of the ith species of ions ($i = 1 - K_\mathrm{ion}$); N_max is the number of electron shells under consideration; K_ion is the number of species of atoms; $R_n^{(i)}$, $I_n^{(i)}$, $C_{mn}^{U(i)}$, $C_{nm}^{D(i)}$, and $A_{mn}^{(i)}$ are the rates of recombination, ionisation, impact excitation and quenching, and radiative decay for the ith species of ions, respectively; N_e is the electron density; $G_n^{(i)} = 1 - P_n^{(i)}/g_n$ is the number of vacancies at the nth level; and g_n is the statistical weight of the nth level.

The laser radiation absorption at the box converter walls is calculated by the Monte-Carlo method (see, for example, [9]). This method is based on the concept of laser beam as a statistical ensemble of a large number of individual rays, each of them propagating according to the laws of geometrical optics. The overall picture of the laser illumination of the inner surface of the box converter in this case is the result of the independent absorption and reflection of individual beams [10]. The points of the LPτ sequence are used as random numbers to accelerate the convergence of the integral sums in the program [9].

The intrinsic surface radiation from each sector is determined by solving the stationary radiation-transport equation [11]

$$(\boldsymbol{\Omega}\nabla)I_\omega = j_\omega - \kappa'_\omega I_\omega, \tag{10}$$

where $I_\omega(\boldsymbol{\Omega})$ is the X-ray intensity in the direction defined by the unit vector $\boldsymbol{\Omega}$; κ'_ω is the absorption coefficient; and j_ω is the emissivity of the substance. Under conditions of thermodynamic equilibrium, the emissivity is defined by the equilibrium intensity (at the given temperature): $j_\omega = \kappa'_\omega I_{\omega\,\mathrm{eq}}$. In the absence of equilibrium, $j_\omega \neq \kappa'_\omega I_\omega$. The results presented in this paper were obtained by using the mean-ion model [12] to find the occupation numbers and the radiation mean free paths in the substance. The solution of Eqn (10) in quadratures can be written in the form

$$I_\omega = \int_0^s j_\omega(s')\exp\left[-\int_{s'}^s \kappa'_\omega(s'')\mathrm{d}s''\right]\mathrm{d}s'. \tag{11}$$

Integration is performed over the coordinate s' in the direction of propagation of radiation from the boundary point $s_0 = 0$ of a luminous object.

The boundary fluxes of X-rays for each sector are calculated by the method of visibility integrals [13] over the calculated intrinsic X-ray luminosity of all the remaining sectors (and are also determined by the external radiation sources specified in the problem). The X-ray intensity at the point $\boldsymbol{r}_i$ from the side of the surface of sector j is

$$I_{\omega ij}^\mathrm{in}(\boldsymbol{r}_i) = \int\frac{I_{\omega j}(\boldsymbol{\Omega}_{ij})\mu_i\mu_j}{|\boldsymbol{r}_i - \boldsymbol{r}_j|^2}\mathrm{d}A_j = \int_{2\pi} I_{\omega j}(\boldsymbol{\Omega}_{ij})\mu_i\mathrm{d}\boldsymbol{\Omega}_j, \tag{12}$$

where $\mu_i = \cos\theta_i$ and $\mu_j = \cos\theta_j$ are the cosines of the angles formed by the vector $\boldsymbol{r}_i - \boldsymbol{r}_j$ with the normals to the surface at the points $\boldsymbol{r}_i$ and $\boldsymbol{r}_j$, respectively; $\boldsymbol{\Omega}_{ij}$ is the unit vector in the direction of the vector $\boldsymbol{r}_i - \boldsymbol{r}_j$; $\mathrm{d}A_j$ is the surface element; and $\mathrm{d}\boldsymbol{\Omega}_j$ is the element of the solid angle.

To calculate the limiting X-ray flux, we must average the intensity in expression (12) over the surface of each sector. Then, the intensity of X-rays incident from the jth sector on the ith sector will be determined by the integral

$$S_{\omega ij} = \frac{1}{A_i}\int I^{\rm in}_{\omega ij}(\boldsymbol{r}_i)\mathrm{d}A_i = \frac{1}{A_i}\int \mathrm{d}A_i \int \frac{I_{\omega j}(\boldsymbol{\Omega}_{ij})\mu_i\mu_j}{|\boldsymbol{r}_i - \boldsymbol{r}_j|^2}\mathrm{d}A_j$$

$$= \frac{1}{A_i}\int \mathrm{d}A_i \int_{2\pi} I_{\omega j}(\boldsymbol{\Omega}_{ij})\mu_i \mathrm{d}\boldsymbol{\Omega}_j, \qquad (13)$$

where A_i is the area of sector i.

We realised the above-formulated approaches in the SND–LIRA software. The results of calculations obtained by using this software are discussed below.

2. Dynamics of radiation fields at the walls of a spherical box

Let us briefly list the main parameters characteristic of most of the experiments performed by the early 1990s [1, 2]. The inner surface of a spherical box converter of diameter 1 mm is illuminated by 12 laser beams introduced through 6 apertures of diameter 600 μm with a relative area of ~0.14. A 1.5-μm thick layer of gold is deposited on the walls of the box. The scheme of experiments is shown in Fig. 1. The laser beams were focused at the centre of the respective apertures by a focusing element of diameter 680 mm and focal length 1100 mm. Therefore, the apex angle of the beam (measured from its axis) was 17.2°. The total energy $E_{\rm L}$ of laser radiation at a wavelength of 1.315 μm introduced into the box was ~9 kJ in these experiments for the pulse FWHM $\tau_{0.5} = 0.35$ ns. It was assumed that the laser radiation power has a Gaussian distribution with a maximum at $t = 1$ ns.

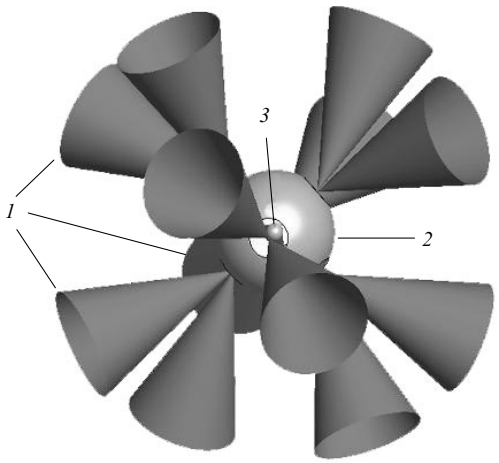

Figure 1. Scheme of experiments with X-ray targets with spherical box converters on the Iskra-5 facility: (*1*) laser beams; (*2*) spherical box; (*3*) capsule filled with a deuterium–tritium mixture.

Figure 2a shows intensity distribution of the laser radiation absorbed at the inner surface of the box converter, obtained in model calculations with the braking absorption coefficient $k_{\rm a} = k_0 \cos^3\gamma$ (where γ is the angle of incidence of radiation at the surface) for $k_0 = 0.5$. The results of calculations show that the 12 beams form quite an intricate pattern of laser illumination on the inner surface of the spherical box. It includes the primary laser spots, extended zones of their overlap and a part of the surface illuminated by scattered laser radiation. Moreover, local spots with a high laser illumination are formed near four apertures due to single and double internal reflection from the spherical surface of the box. Estimates obtained by taking into account the nonuniform plasma spread at the box walls show that such spots may persist for about half the laser-pulse duration.

Analysis shows that in the general case 25 regions can be distinguished on the inner surface of the box in which the absorption of laser radiation differs considerably (see Fig. 2). These include 12 primary laser spots plus 8 regions of their pairwise overlap, regions of high local illumination near four apertures, and the remaining part of the inner surface located outside by the primary laser illumination zones.

X-rays emitted by the box walls are generated in different layers of plasma near the walls and have different parameters. Absorption of high-intensity laser radiation leads to the formation of a hot and low-density laser corona, which is the source of highly nonequilibrium primary X-rays (with a line spectrum). The primary X-

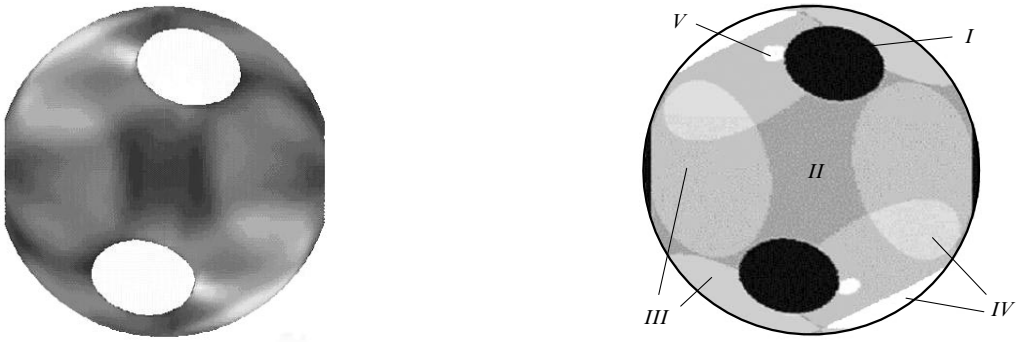

Figure 2. (a) Intensity distribution of absorbed laser radiation (shown in shades of grey) at the inner surface of a spherical box calculated for the braking absorption coefficient $k_{\rm a} = k_0 \cos^3\gamma$ with $k_0 = 0.5$ and (b) sector division of the spherical box: (*I*) aperture for introducing laser radiation (sector 0); (*II*) part of the inner surface of the box not covered by primary spots (sector 1); (*III*) areas illuminated by a single laser beam (sectors 2–4); (*IV*) area of pairwise overlapping of laser spots (sectors 5 and 6); (*V*) zones of high local laser illumination located near the four apertures (sector 7).

rays penetrate the layers of a colder and denser plasma (X-ray corona region) where quasi-equilibrium X-rays with an effective temperature of about 200 eV are generated [14].

In the case of a spherical box, the geometrical visibility factors $\mu_i\mu_j/|\boldsymbol{r}_i - \boldsymbol{r}_j|^2$ in the kernel of integral operators (12) and (13) are equal to $1/(4R^2)$ (R is the box radius) and are independent of $\boldsymbol{r}_i$, $\boldsymbol{r}_j$. For this reason, any element of the spherical surface emitting radiation inside the sphere according to the Lambert law (which holds for an optically dense emitter) uniformly illuminates all regions of the inner surface of the box. Therefore, for a spherical box, all the points on its inner surface are under identical conditions for the incident X-rays, and any difference in them is caused only by different absorption of laser radiation. Hence, only the difference in laser illumination should be taken into account while dividing the spherical surface of a converter box into sectors.

As mentioned above, the surface of the box was divided into 25 regions (sectors) in our calculations. If laser beams have equal energies, some of these sectors prove to be under identical conditions and can therefore be combined together. In this case, the number of sectors required for calculations can be reduced to seven. Figure 2b shows the arrangement of sectors on the box surface. One can see that sector 0 combines regions of apertures for introducing laser radiation, sector 1 contains part of the surface outside laser spots, which is illuminated only by scattered radiation, sectors 2–4 are the regions illuminated by a single laser beam, sectors 5 and 6 are the regions illuminated simultaneously by two laser beams, while sector 7 contains four local zones strongly illuminated by lasers in the vicinity of four apertures. The sizes of the sectors and the integrated radiation fluxes corresponding to them are presented in Table 1. Thus, the arrangement of the sectors is determined by the pattern of illumination of the inner surface of the box by laser radiation. The geometry of laser sources in the illumination pattern of the target has a symmetry of rotation only through 180° and reflection symmetry relative to the equatorial plane and rotation through 90°. Therefore, the laser illumination structure on the box surface is highly asymmetric.

We will analyse the conditions at the inner surface of the box by assuming that all laser beams have the same energy. One can see from Table 1 that the contributions from the regions singled out by us in the vicinity of the apertures (where the laser radiation is concentrated due to successive reflections from the inner surface of the spherical mirror) is quite small. Hence these regions do not have a noticeable effect on the generation of X-rays inside the box.

In all sector calculations, we solved the spherical gas-dynamic problem. The boundary conditions for the radiation fluxes were specified at the inner surface of the box (the outer surface is assumed to be the free boundary). Limiting X-ray fluxes were calculated for each spectral region. Laser radiation is reflected at the point of its reversal near the critical plasma surface (see, for example, [15]). The main part of the incident laser radiation energy is also absorbed at this point. Generation and absorption of laser radiation takes place in the region where the optical density $\kappa'_\omega \Delta r$ of the substance becomes comparable to unity. Our calculations showed that during the time period $t \leqslant 1.3$ ns, which is interesting from the point of view of the target operation, the displacement of the critical plasma surface on the walls of the spherical box does not exceed 100–150 μm (for the initial radius $R = 1.0$ mm). The displacement of plasma layers in which the optical density $\kappa'_\omega \Delta r \sim 1$ is even smaller. Thus, the geometry of the problem can be assumed fixed during calculations of the limiting radiation fluxes.

Table 1. Total energy balance in sectors for the same energy of all laser beams at the instant $t = 1.4$ ns.

Sector number	$\Delta\Omega/4\pi$	E_L/kJ	E_X/kJ	Q_X/kJ
0	0.1382	2.850	0.964	–
1	0.1530	0.700	1.062	0.977
2	0.2202	1.590	1.530	1.700
3	0.1275	1.095	0.885	1.080
4	0.2211	1.620	1.535	1.720
5	0.0629	0.795	0.437	0.679
6	0.0720	0.820	0.501	0.723
7	0.0048	0.082	0.034	0.060
Total	1	9.560	6.950	6.940

Note: E_L is the energy of absorbed laser radiation; $\Delta\Omega$ is the solid angle at which the surface of the sector is seen from the centre of the box; E_X is the energy of X-rays incident on the surface of a given sector from all the remaining sectors; and Q_X is the energy emitted by the surface of the given sector.

Figure 3a shows the intensities of laser radiation absorbed at the surface of sectors 1–7 at different instants of time, while Fig. 3b shows the limiting X-ray fluxes integrated over the spectrum (negative values indicate that energy is emitted at these sectors of the inner box surface).

The effective temperature of X-rays generated at the surface of each of the seven sectors is shown in Fig. 4. The solid curve in the figure shows the temperature of radiation emerging from the apertures. One can see that all sectors can be combined into three groups near the laser pulse maximum ($t = 1$ ns) and especially at the subsequent instants. The maximum of the radiation temperature is achieved at $t = 1.10 - 1.15$ ns and amounts to 190–195 eV in the region of primary spots, while its value in the overlap region of the spots is 200–205 eV. The surface of the box illuminated by scattered laser radiation is heated to ~180 eV (the maximum temperature of radiation incident on the surface is ~185 eV). We will take into account this circumstance and will present below the results related only to one of the sector calculations for each group.

Figure 5 shows the absorption coefficient $\bar{k}_a$ averaged over all angles of incidence of laser radiation at various instants of time for sectors 1, 2 and 5. One can see that it has a minimum at $t = 0.8 - 0.9$ ns and then increases monotonically (the laser pulse has a maximum at $t = 1.0$ ns).

Consider now the theoretical parameters of X-rays in a spherical box. Figure 6 shows the spectral fluxes emitted by the surfaces of sectors 1, 2 and 5 in the region of the maximum emission of the inner surface of the box ($t = 1.1$ ns). About 10 % of the energy emitted by the box converter walls are contained in the hard X-ray line region between 2.3 and 3 keV. The results of calculations show (see Table 1) that only about 14 % of the total X-ray energy emitted by the box walls emerge through the apertures, i.e. the radiation losses at the apertures are determined by the relative area of the apertures.

Figure 7 shows the X-ray in various regions of the inner surface of the box at the maximum of the X-ray spectrum (0.6–0.7 keV) and in the hard X-ray spectral region (2.5–2.6 keV) at the instant 1.1 ns.

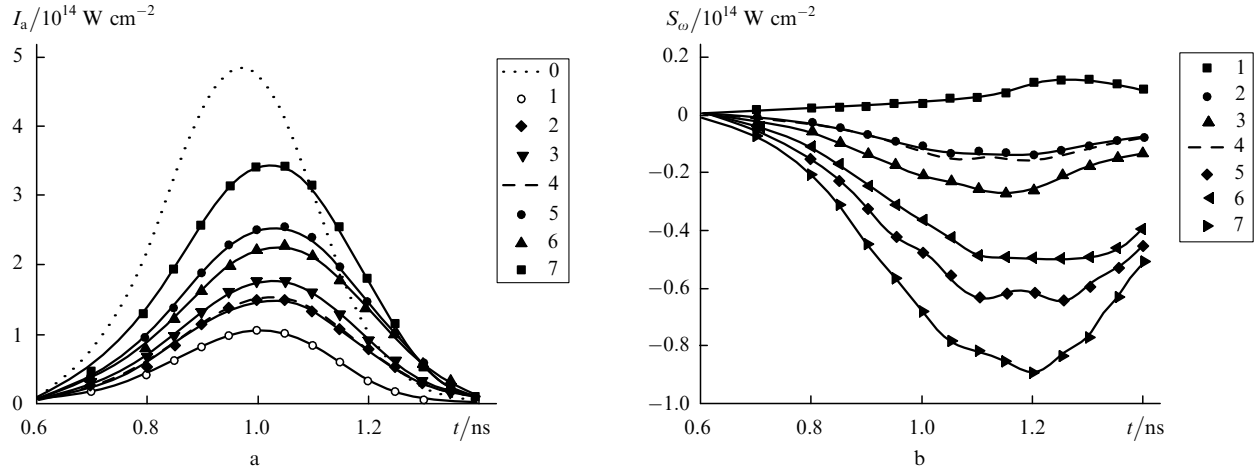

Figure 3. Limiting radiation fluxes at the inner surfaces of sectors 0–7 at various instants: (a) the intensity of absorbed laser radiation and (b) X-ray fluxes I_a integrated over the spectrum.

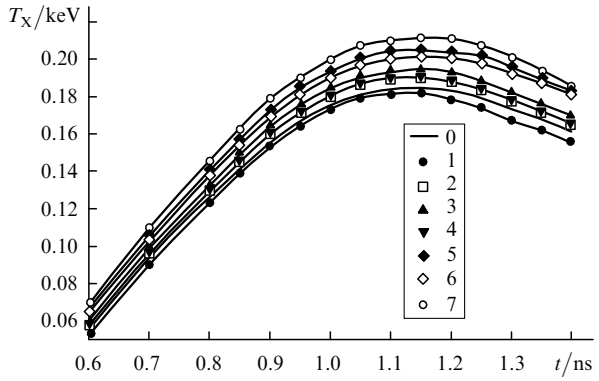

Figure 4. Effective temperatures T_X of X-rays generated at the surface of sectors 1–7 and the temperature of X-rays emerging from the box through the aperture (sector 0) at various instants.

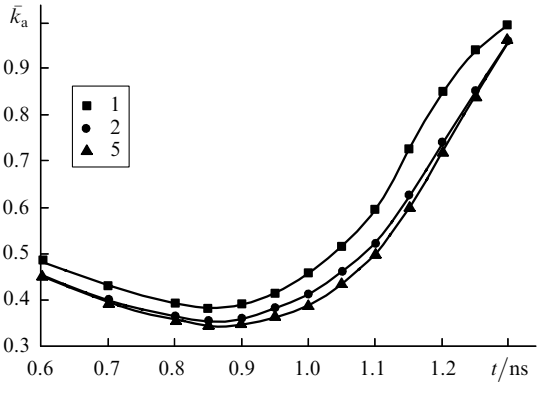

Figure 5. Averaged (over all angles of incidence) absorption coefficient $\bar{k}_a$ of laser radiation at the surface of sectors 1, 2, 5 at various instants.

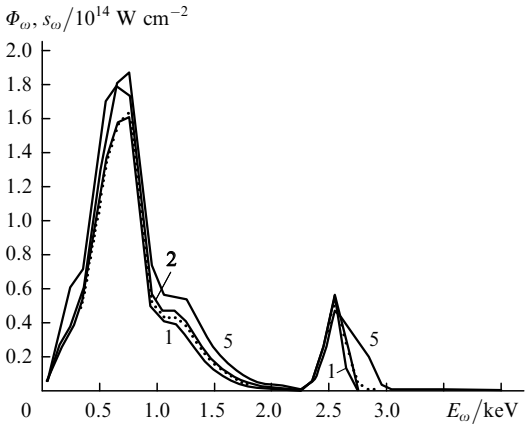

Figure 6. X-ray fluxes Φ_ω emitted by the surface of sectors 1, 2, 5 (solid curves) and the flux s_ω emerging through the apertures (dotted curve) at the instant close to the maximum emission ($t = 1.1$ ns).

3. Homogeneity of X-ray irradiation of the capsule

Consider now the uniformity of X-ray irradiation of the central capsule. The results of calculations of the X-ray luminosity of the box walls were used to calculate the root-mean-square inhomogeneity ε_{rms} of the X-ray flux incident on a spherical surface of diameter 280 μm, which is equal to the initial diameter of the capsule. Figure 8 shows the inhomogeneity ε_{rms} in various spectral regions at the instant $t \approx 1.1$ ns (for laser beams of the same energy and for two versions of the energy spread in laser channels in the experiments carried out on 06.11.1992 and 26.11.1992), when the luminosity of the box walls was maximal. One can see that the uniformity of irradiation of the capsule is different in different spectral regions. Thus, for laser beams of the same energy at the maximum of the spectrum (0.5–0.8 keV), the nonuniformity of irradiation is less than 2 %, while at the descending region of the spectrum (0.9–1.5 keV), its value is 2.2 %–3.5 %, and, for the hard X-ray spectral line region (2.7–2.9 keV), the nonuniformity increases to about 20 %. Note that the radiation energy in the latter spectral region is quite low. Of the total energy emitted by the inner surface of the box, only about 0.3 % falls in this interval. (However, inhomogeneity in this spectral region may lead to observable consequences due to the high penetrability of radiation.) The root-mean-square inhomogeneity of the X-ray irradiation of the capsule was estimated by the Monte-Carlo method as $\varepsilon_{rms} \approx 2$ % [10]. One can see that this estimate is confirmed for the main part of the spectrum. An abrupt increase in the irradiation inhomogeneity in the region 2.7–2.9 keV is caused by the emission of the regions of overlapping of primary spots of

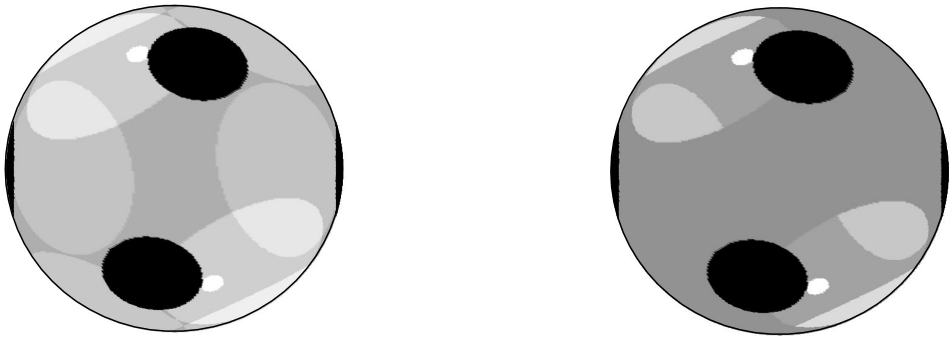

a b

Figure 7. Energy emitted per unit time in the spectral intervals (a) 0.6 – 0.7 keV and (b) 2.5 – 2.6 keV by the spherical box wall at the instant $t = 1.1$ ns. The shades of grey correspond to various intensities of emission (black corresponds to zero emission intensity).

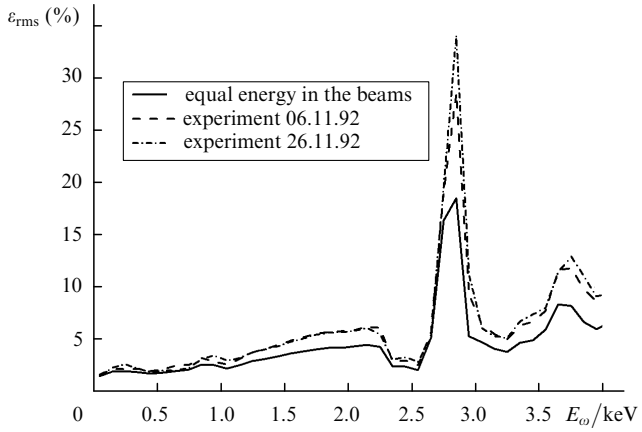

Figure 8. Root-mean-square inhomogeneity ε_{rms} of X-ray irradiation of the capsule in various spectral regions for the maximum luminosity of the box walls ($t = 1.1$ ns).

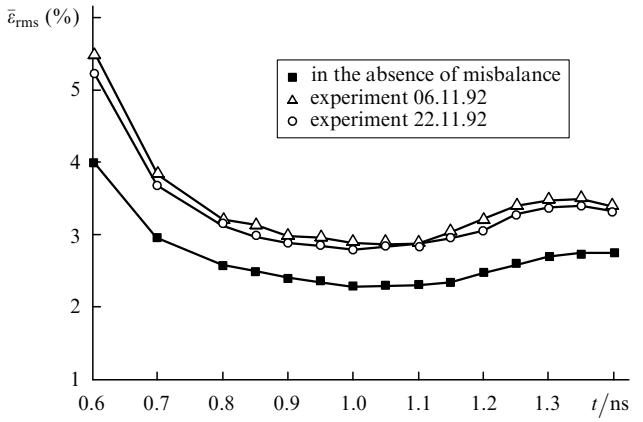

Figure 9. Root-mean-square inhomogeneity $\bar{\varepsilon}_{\text{rms}}$ of the X-ray field at the surface of the capsule at various instants.

two laser beams (sectors 5 and 6), which is not compensated in this spectral region by emission from other parts of the inner surface of the box. The data presented in Fig. 6 illustrate this result.

Let us calculate the inhomogeneity of irradiation of the capsule averaged over the spectrum. For this purpose, we proceed as follows. Let $\bar{I}_{\text{X}}(\omega)$ be the X-ray spectral intensity averaged over the capsule surface. We define the average inhomogeneity as

$$\bar{\varepsilon}_{\text{rms}} = \frac{\int_0^\infty \bar{I}_{\text{X}}(\omega)\varepsilon_{\text{rms}}(\omega)\mathrm{d}\omega}{\int_0^\infty \bar{I}_{\text{X}}(\omega)\mathrm{d}\omega}. \tag{14}$$

The advantage of such a definition of $\bar{\varepsilon}_{\text{rms}}$ is that contribution from various spectral regions to (14) is proportional to the energy of X-rays in these regions.

Figure 9 shows the root mean square inhomogeneity (14) at various instants. For the same energy of beams in the interval $0.8 \leqslant t \leqslant 1.2$ ns, the X-ray field inhomogeneity on the capsule lies in the range 2.3 % – 2.5 % and increases to 2.7 % for $t = 1.3$ ns. The variation in $\bar{\varepsilon}_{\text{rms}}$ is caused by the difference in the dynamics of luminosity of the regions irradiated by one laser beam (sectors 2 – 4), regions illuminated simultaneously by two beams (sectors 5 and 6), and the rest of the inner surface of the box illuminated by the scattered laser radiation (this can be seen clearly in Fig. 4). The consideration of energy misbalance (different energies in the beams) introduces an inhomogeneity of ~3 % in the main part of the X-ray pulse ($t = 0.8 - 1.2$ ns) generated in the box, and ~3.5 % at later instants.

It is convenient to introduce partial inhomogeneities ε_j to characterise the spatial inhomogeneities of various scales existing in the X-ray field at the capsule surface. The partial inhomogeneities are expressed in terms of the amplitudes of the expansion of distribution of the intensity $I_{\text{X}}(\theta, \varphi)$ of the X-rays incident on the capsule in spherical harmonics $Y_{jm}(\theta, \varphi)$, and are connected with the root-mean-square inhomogeneity through the relation (see [10] for details)

$$\varepsilon_{\text{rms}} = \left(\sum_{j=1}^{\infty} \varepsilon_j^2 \right)^{1/2}. \tag{15}$$

The partial inhomogeneities ε_j do not vary upon rotation of the coordinate system and are therefore convenient parameters of the 'spectrum' of spatial nonuniformities of irradiation of the capsule. Figure 10 shows the partial inhomogeneities ε_1, ε_2, ε_3, and ε_4 associated with various spatial scales for the same laser beam energy (in this case, $\varepsilon_1 = 0$) and taking into account the energy misbalance observed in one of the experiments. The descending order of partial inhomogeneities ($\varepsilon_2 \geqslant \varepsilon_3 \geqslant \varepsilon_4$) reflects the pro-

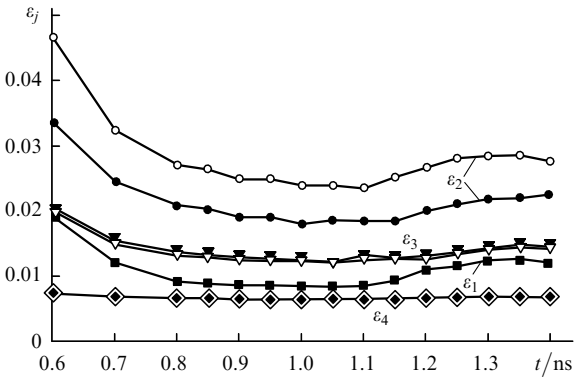

Figure 10. Partial inhomogeneities ε_j of the X-ray field at the surface of the capsule at various instants, calculated for laser beams of equal energy (dark symbols) and by taking into account the energy misbalance for the experiment conducted on 06.11.92 (light symbols).

perty of smoothing of inhomogeneities during transport of X-rays from the box walls to the capsule: the smoothing increases sharply with the harmonic number j; harmonics with $j > 5$ are practically nonexistent. One can see from Fig. 10 that the first-order harmonic acquires a nonzero amplitude (ε_1 becomes nonzero) when we take into account the fact that the beam energies are not equal. In this case, a slight increase in the amplitudes of the second-order harmonics is also observed, while the amplitudes of third- and higher-order harmonics remain almost unchanged.

References

1. Abzaev F.M., Bel'kov S.A., Bessarab A.V., Bondarenko S.V., et al. *Zh. Eksp. Teor. Fiz.*, **114**, 1993 (1998).
2. Belkov S.A., Abzaev F.M., Bessarab A.V., et al. *Laser and Particle Beam*, **17** (4), 591 (1999).
3. Murakami M., Meyer-ter-Vehn J. *Nuclear Fusion*, **31**, 1315 (1991).
4. Tsakiris G.D. *Phys. Fluids*, **4** (4), 992 (1992).
5. Srivatsava M.K., Kumar Vinod, Menon S.V.G. *Phys. Plasmas*, **7** (6), 2616 (2000).
6. Pakula R., Sigel R. *Phys. Fluids*, **28** (1), 232 (1985).
7. Schnittman J.D., Craxton R.S. *Phys. Plasmas*, **7** (7), 2964 (2000).
8. Dolgoleva G.V. *Vopr. Atom. Nauk. Tekhn. Ser. Metod. Program. Chislen. Reshen. Zadach Mat. Fiz.*, (21), 29 (1983).
9. Sobol' I.M. *Chislennye metody Monte Karlo* (Numerical Monte-Carlo Methods) (Moscow: Nauka, 1973).
10. Bondarenko S.V., Kochemasov G.G. *Proc. First Int. Conf. on Inertial Fusion Science and Application (IFSA'99)* (Bordeaux, France, 1999) p. 166.
11. Zel'dovich Ya.B., Raizer Yu.P. *Fizika udarnykh voln i vysokotemperaturnykh gazodinamicheskikh yavlenii (*Physics of Shock Waves and High-temperature Gas-dynamic Phenomena) (Moscow: Nauka, 1966).
12. Bel'kov S.A., Dolgoleva G.V. *Vopr. Atom. Nauk. Tekhn. Ser. Matemat. Mode. Fiz. Protses.*, (1), 59 (1992).
13. Babaev N.N., Bazhenov S.V., Bazin A.A., Vasina E.G., Gorev V.V., Dement'ev Yu.A., Zagrafov V.G., Karpovtsev E.L., Kirillov L.I., Mironova V.F., Pevnaya P.I., Perepelkin P.A., Skidan G.I., Sofronov I.D., Tikhomirov B.P., Tikhomirova E.N., Yurina N.I. *Vopr. Atom. Nauk. Tekhn. Ser. Matemat. Mode. Fiz. Protses.*, (4), 3 (1995).
14. Mkhitarjan L.S., Kochemasov G.G. *Proc. 23th Europian Conf. on Laser Interaction with Matter (ECLIM)* (London, England, St John's College, 1994).
15. Landau L.D., Lifshitz E.M. *Electrodynamics of Continuous Media* (Oxford: Pergamon Press, 1984; Moscow: Nauka, 1992).